Bioprinting 28 (2022) e00240

Contents lists available at ScienceDirect

Bioprinting

journal homepage: www.sciencedirect.com/journal/bioprinting

Spatially guided endothelial tubulogenesis by laser-induced side transfer (LIST) bioprinting of HUVECs

Hamid Ebrahimi Orimi [a,b], Erika Hooker [a,c,d], Sivakumar Narayanswamy [b], Bruno Larrivée [a,c,d], Christos Boutopoulos [a,c,e,*]

[a] Centre de Recherche Hôpital Maisonneuve-Rosemont, Montréal, Canada
[b] Department of Mechanical, Industrial and Aerospace Engineering, Concordia University, Montréal, Canada
[c] Department of Ophthalmology, Faculty of Medicine, University of Montreal, Montréal, Canada
[d] Department of Molecular Biology, University of Montreal, Montreal, Quebec, Canada
[e] Institute of Biomedical Engineering, University of Montreal, Montreal, Quebec, Canada

ARTICLE INFO

Keywords:
Laser-induced side transfer
Drop-on-demand
Bioprinting
Angiogenesis
Lumen formation
Bone morphogentic protein 9 (BMP9)
Laser-assisted bioprinting

ABSTRACT

The ability to bioprint microvasculature networks is central for drug screening and for tissue engineering applications. Here we used a newly developed bioprinting technology, termed laser-induced side transfer (LIST), to print human umbilical vein endothelial cells (HUVECs) and to spatially guide endothelial tubulogenesis. We investigated the effect of three bioprinting matrices (fibrin, Matrigel and Matrigel/thrombin) on HUVECs self-assembly. Furthermore, we studied the effect of pro- and anti-angiogenic compounds on sprouting angiogenesis and tubulogenesis. We found that HUVECs self-assembly is optimal on Matrigel/thrombin due to the formation of fibrin stripes that enhance HUVECs confinement and adhesion. Importantly, we showed that treatment of printed HUVEC lines with the anti-angiogenic factor bone morphogenetic protein 9 (BMP9) significantly improves the percentage of lumen coverage. Our results showcase LIST as a powerful bioprinting technology to study tubulogenesis and to screen compounds targeting microvasculature pathologies.

1. Introduction

Bioprinting technologies aim to build living constructs with long term mechanical and biological stability suitable for transplantation, as well as to provide improved 3-dimensional (3D) drug discovery models [1,2]. Bioprinting of human umbilical vein endothelial cells (HUVECs) is the basis for creating capillary networks, which are of great interest for a variety of applications. Bioprinted living constructs of clinically relevant size require the incorporation of a fine-printed (resolution 100–200 μm) HUVECs capillary network ("capillary bed") to ensure cell access to nutrients and oxygen as well as removal of metabolic wastes. This is essential for the survival of the printed constructs in the long term [3–5]. Furthermore, bioprinted microvasculature can serve as a platform to study tubulogenesis and to screen drugs before initiating animal studies.

A central goal in bioprinting is the precise positioning of multiple cell types and/or biomaterials on a supporting substrate. Convectional bioprinting technologies include drop-on-demand (DOD) approaches, such as ink-jet printing [6–9] and laser-induced forward transfer (LIFT) [10], as well as microextrusion-based bioprinting (MBB) [2,11]. Depending on the printing mechanism, these technologies present only partial compatibility with bioink formulations, with bioink viscosity being the limiting factor [2]. MBB have been used to create vascular networks [12–18]. Yet, the printing resolution in MBB is not suitable for fine printing of microvascular networks. DOD bioprinting (e.g., inkjet [19,20] and laser-induced forward transfer (LIFT) [21–26]) is an alternative approach for direct printing of HUVECs that attains finer spatial resolution compared to MBB [2]. Our lab has developed a laser-based DOD bioprinting technique, termed Laser Induced Side Transfer (LIST). LIST can be used to print primary cells such as HUVECs and neurons without compromising cell functionality [27,28]. LIST printed HUVECs maintain the ability to proliferate, migrate and to form intercellular junctions [27].

The printing matrix has a predominant effect on the self-organization of printed HUVECs. Matrigel immersed polyester urethane urea cardiac patches [24] and collagen [21,25] have been previously used as matrices. LIFT printed HUVECs on Matrigel self-assembled in cord-like formations [23,25]. However, lumen formation was not sufficiently documented in those early studies. LIFT printed HUVECs form similar

* Corresponding author. Department of Ophthalmology, Faculty of Medicine, University of Montreal, Montréal, Canada.
E-mail address: christos.boutopoulos@umontreal.ca (C. Boutopoulos).

https://doi.org/10.1016/j.bprint.2022.e00240
Received 17 June 2022; Received in revised form 4 August 2022; Accepted 19 August 2022
Available online 29 August 2022

cord-like formations on collagen [26]; however lumen formation has yet to be demonstrated. Pro- and anti-angiogenic factors modulate the microvasculature *in vitro* and *in vivo* [29,30]. Several 3D angiogenesis assays including tissue explants embedded in gels or isolated endothelial cells grown in gels can mimic the *in vivo* environment, where endothelial cells surrounded by matrices can form tube-like structures in response to growth factors. These assays allow for rapid evaluation of angiogenic effects of growth factors but are limited to random network formation. The ability to bioprint spatially controlled capillary networks in a reproducible manner can address this limitation and can open new possibilities for studying tubulogenesis and for screening drugs for microvasculature pathologies.

Here we used the newly developed LIST to bioprint HUVECs networks on Matrigel, Fibrin and Matrigel/thrombin. We sought to investigate which matrix can better support guided tubulogenesis. We used microscopy to study HUVECs self-assembly post printing as well as an image processing algorithm to quantify lumen formation in printed HUVECs patterns. Finally, we exploited printed patterns as an assay to evaluate the effect of pro- and anti-angiogenic compounds on sprouting angiogenesis and tubulogenesis.

2. Materials and methods

2.1. Bioink preparation

HUVECs (Promocell) were cultured in EndoGRO-VEGF medium (Millipore). The bioink formulation consisted of HUVECs (18.75×10^6 per ml) suspended in Basal medium (SCME-BM, Millipore), supplemented with fibrinogen (13.1 μM) (F8630-5G; Sigma-Aldrich) and aprotinin (6.92 μM) (10820–25 MG; Sigma-Aldrich) and a red food dye Allura red AC (10 mM) (458848-100G, Sigma-Aldrich). The dye enhances light absorption by the bioink and facilitates printing at relatively low energy per laser pulse. In fact, the droplet generation threshold is ~80 μJ per pulse for the beam delivery system (see 2.4) used in our study. When no light absorbing material is used, ~15-fold higher energy per pulse (1.25 mJ) is needed to generate a bubble using the same system [31]. Such a high energy is not suitable for printing because it causes thermomechanical stress that can damage both the bioink and the capillary.

2.2. Live-dead assay for red dye cytotoxicity assessment

We used a trypan blue exclusion test to assess potential cytotoxicity effects of the Allura red dye. HUVECs were exposed to Allura red (10 mM or 50 mM in culture medium) for 50 min, corresponding to the typical exposure time during a bioprinting experiment. The samples were washed, and fresh medium was added. Trypan blue was used to assess viability 1-, 2- and 3-days post exposure to the dye.

2.3. Matrices

We prepared all gels on 18 mm × 18 mm microscope cover glasses (12-545-A, Fisher Scientific). For fibrin substrates, we used 314 μL of a Basal medium (SCME-BM, Millipore), containing fibrinogen (14.11 μM) (F8630-1G, Sigma), aprotinin (7.45 μM) (10820-25 MG; Sigma-Aldrich) and 10 μL of a thrombin solution (3.09 U/mL final concentration in the fibrin gel) (T7513- 100UN, Sigma-Aldrich). We used drop-casting to deposit the two solutions onto the microscope cover glasses 1 h before printing. For Matrigel/thrombin substrates, 100 μL Matrigel (#35623, Corning) was thawed at room temperature and mixed with 5 μL thrombin (4.76 U/mL final concentration in Matrigel) (T7513-100UN, Sigma Aldrich). The mixtures were drop-casted on cover glasses, which were then placed in an incubator (5% CO2 at 37 °C) for 3 h. For Matrigel substrates, we used the same protocol without adding thrombin.

2.4. Printing setup and protocol

HUVECs were printed using a setup the has been previously described in detail [27]. Briefly, the gel-coated substrates were mounted on a motorized XYZ translation stage. A microcapillary (Vitrocom hollow square capillary, 0.3 mm inner dimension, 0.15 mm wall thickness and 50 mm long) was brought close (~500 μm) to the gel. The bioink was loaded to the microcapillary via a syringe pump (NE-1000, New Era Pump Systems Inc.). To eject bioink drops, we focused a nanosecond (ns) pulsed laser (Ultra compact pulsed Nd:YAG, Nano L series, wavelength 532 nm, pulse duration: 6 ns) in the middle of the microcapillary and 500 μm far from its distal end using a 4X Olympus plan achromat objective. The laser energy at the sample level was 110 μJ. Usually, four 10 mm-long line patterns were printer per sample. After printing, the samples were placed into an incubator for 10 min. Next, medium was added. The medium was changed after 30 min to remove the diffused red dye.

2.5. Rheology

We measured the storage modulus (G') and loss modulus (G") of the hydrogels using a Discovery, Hybrid-2rheometer (TA Instruments, New Castle, DE, USA). 25 μl drops of hydrogels were added to the fixed plate resulting to circular samples ~8 mm in diameter and ~1 mm in thickness. The temperature was set to 37 °C for Matrigel and Matrigel/Thrombin samples, whereas room temperature was used for Fibrin. The hydrogels were compressed by axial force and the applied oscillation strain ranged from 0.1 to 500% using an angular frequency of 10 rad/s. The average of storage and loss moduli was calculated for the storage range between 0.1 and 50% where the rheology presents plateau regimes in all matrices.

2.6. Post printing cell viability

LIST-printed cells were stained with Hoechst 33342 (14.237 μM) (14533–100 MG; Sigma-Aldrich) Calcein AM (0.402 μM) (400146, Cayman chemical). Hoechst 33342 stained all cells, whereas Calcein AM stained live cells only. We obtained fluorescence images of printed cells 0-, 1- and 3- days post printing using an inverted motorized microscope (Zeiss AxioObserver Z1). We used a built in MATLAB algorithm to process the images. The algorithm segments individual cells using Hoechst 33342 staining and registers the intensity of the colocalized green channel (Calcein AM). The fluorescence signal threshold to consider a cell live was set to $I_b+5 \times \sigma_{Ib}$, where I_b and σ_{Ib} are the background green channel intensity and its standard deviation, respectively.

2.7. Immunofluorescence imaging

We used immunofluorescence to visualize intercellular junctions for LIST-printed HUVECs at day 5 post printing. We first incubated the samples with PFA 4% for 10–15 min to fix the cellular protein and subcellular structures in place. The samples were then incubated with a blocking solution containing 3% BSA and 0.1% Triton X-100 in PBS (including Mg_2^+ and Ca_2^+) for 10–15 min to induce permeabilization. Samples were then incubated with CD31 (550389; BD Biosciences; 1:500) antibodies diluted in permeabilization medium at 4 °C in the dark overnight. The following day, the samples were washed and incubated with Alexa488 labeled-goat anti-mouse IgG (cat# A32723; Thermo Fisher; 1:1000) and then treated with DAPI (1:2000). Finally, the samples were imaged by an upright confocal microscope (Zeiss AxioExaminer Z1).

2.8. Lumen segmentation and quantification

We developed a MATLAB algorithm to quantify lumen formation in

printed HUVECs lines. We binarized fluorescence images (i.e., z-stack frames) to detect connected HUVECs using a thresholding approach detailed in the provided MATLAB code. For each z-stack frame the algorithm calculates the void area contained between connected HUVECs in both x and z axes. Note that lines are printed along the y axis. Void areas $<25\ \mu m^2$ or having length $<75\ \mu m$ along the y axis, or those that do not repeat in at least five consecutive slices (i.e., 4 μm thickness) were rejected. We summed the length of the remaining segmented areas per z-stack frame and used the frame with the largest value to report lumen length. The MATLAB code can be found in the Supplementary material.

2.9. Sprouting angiogenesis assays

In each well of a 24-well plate, we combined 12 μL of a thrombin solution (1 U/mL final concentration in the fibrin gel) (T7513- 100UN, Sigma-Aldrich) and 50 μg/ml aprotinin (10820-25 MG; Sigma-Aldrich) with 400 μL of fibrinogen (2.5 mg/ml, final concentration of 7.28 μM) dissolved in basal medium (SCME-BM, Millipore). To induce gelation, we placed the well in a 37 °C incubator for 30 min. Next, we added 400 μL fibrinogen containing HUVECs (~2.5×10^5 cell per well) on top of the solid fibrin layer in each well and placed them in a 37 °C incubator for an hour to allow gelation. Then we added 400 μL of complete media (EndoGRO-Millipore) containing IMR90 fibroblasts (~2.5×10^5 cell per well). The next day (Day 1), we treated the cells with pro- and anti-angiogenic factors and monitored sprout formation on a daily basis. For fluorescence imaging, we removed the fibroblasts using 0.5% trypsin and stained the HUVECs with 4 μg/ml Calcein AM (400146, Cayman chemical).

2.10. Anti- and pro-angiogenic treatments

Sprouting HUVEC samples were treated with either anti-angiogenic recombinant human BMP9 protein (10 ng/ml) (3209-BP-010/CF, R&D Systems) or FLT1-FC (500 ng/ml) (7756-FL-050, R&D Systems) in complete endothelial media (CM). In order to establish conditions where pro-angiogenic factors could promote sprouting, pro-angiogenic compounds BMP6 (200 ng/ml) (120-06, Peprotech Inc) or VEGF (25 ng/ml) (293-VE-010, R&D Systems) were added to HUVECs in basal endothelial media supplemented with 2% FBS. Both pro- and anti-angiogenic treatments were added 1-day after printing or after seeding (conventional assays). As BMP9 has been reported to circulate at concentrations between 2 and 12 ng/ml in humans [32], and given that studies, including our own, have shown that the activity of BMP9 reaches a plateau at around 10 ng/ml [33–35], subsequent experiments were performed using this concentration. Complete endothelial growth medium and basal endothelial medium supplemented with 2% FBS were used as controls for anti- and pro-angiogenic treatments, respectively. Every other day, the medium was changed, and the treatments were repeated.

2.11. Statistical analysis

Results are expressed as mean ± standard deviation in all experiments. Statistical significance was tested by one-way or two-way analysis of variance (ANOVA). ANOVA is a statistical model that analyzes differences among means when the effect of one or multiple factors is investigated [36]. We used GraphPad 8.1 for statistical analysis and graph preparation.

3. Results

3.1. Droplet and line printing by laser-induced side transfer

LIST is a drop-on-demand printing technology that uses focused laser pulses to eject bioink drops from a glass microcapillary towards a receiving substrate (Fig. 1a). The high-power density of the laser pulse at focus leads to a series of phenomena, including local ionization of the bioink, micro-bubble generation, liquid displacement, jet formation, and jet impingement at the substrate [27]. Fig. 1a shows a schematic representation of the LIST working principle and indicative high-speed imaging of droplet ejection. LIST can be used to print arrays of cell-laden drops or continuous lines with appropriate adjustment of the overlap among adjacent droplets.

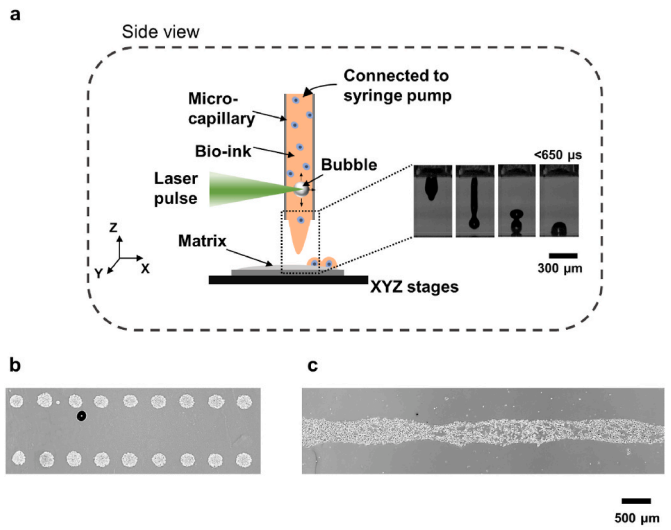

Fig. 1. (a) Schematic showing the LIST bioprinting process and indicative high-speed imaging of droplet ejection. (b) An array of LIST-printed HUVECs-laden droplets (c) A LIST-printed line using 20% overlap between adjacent droplets.

LIST uses a food dye additive (10 mM Allura red) in the bioink to enhance light absorption at 532 nm. We validated potential cytotoxicity effects of the dye on HUVECs at 10 mM and 50 mM (i.e., 5-fold higher than the one used in the bioink), using a viability assay. We found no compromise in the cell viability for a 0-, 1-, and 3-days post-exposure (Fig. S1).

In this work we performed printing using a previously optimized laser pulse energy of 110 μJ per pulse [27]. An array of HUVEC-laden droplets is shown in Fig. 1b. A 200 μm distance between adjacent droplets (20% overlap) was used to print continuous lines (Fig. 1b).

3.2. The effect of the support matrix on HUVECs viability, self-assembly, and adhesion

After establishing a protocol for printing continuous lines, we sought to investigate the effect of the support matrix on HUVECs viability, self-assembly, and adhesion. To do so, we printed HUVECs (18.75×10^6 HUVECs/mL in a bioink consisting of EBM-2 supplemented with fibrinogen, aprotinin and Allura red AC) lines on Fibrin-, Matrigel- and Matrigel/thrombin-coated substrates. For all substrates, we found that LIST-printed HUVECs present high viability, ranging from 90.9% to 99.6% and that there is no significant difference on the cell viability for the different matrices (Fig. S2). Furthermore, we did not observe loss of cell viability compared to controls for 0-, 1- and 3- days post printing (Fig. S2). Note that Matrigel/thrombin and Matrigel-substrates had similar storage (Matrigel/thrombin, G': 6.499 kPa, Matrigel, G': 5.622 kPa) and loss modulus (Matrigel/thrombin, G": 0.936 kPa, Matrigel, G'': 0.899 kPa) and were relatively stiff compared to fibrin substrates (G': 0.360 kPa, G'': 0.086 kPa) (Fig. S3).

Fibrin substrates contained excess thrombin that catalysed gelation of bioprinted cell-laden drops via conversion of fibrinogen to fibrin. Yet, HUVECs proliferated on fibrin without preserving the initial footprint of the printed lines. Two days after printing the cells invaded the available surface of the matrix (Fig. 2a). We observed similar behaviour in a control experiment, involving conventional seeding of HUVECs on fibrin

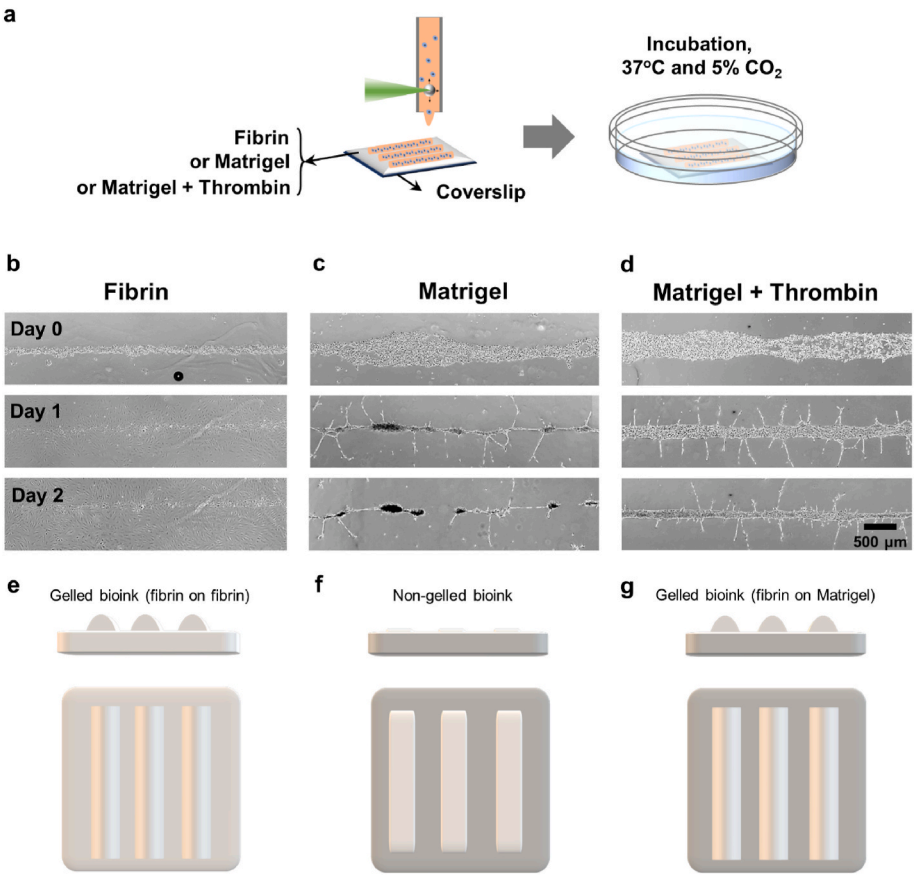

Fig. 2. (a) Schematic of LIST-printing of HUVECs lines on different matrices; two days post-printing observation of LIST-printed HUVECs with optical microscopy shows (b) non-directional HUVECs proliferation on fibrin-coated substrate, (c) cord-like HUVECs self-assembly on Matrigel-coated substrate combined with poor adhesion and sprouting, and (d) cord-like HUVECs self-assembly on Matrigel/Thrombin-coated substrate combined with strong adhesion and sprouting. (e)–(g) Schematic representation of the bioprinted patterns for the different matrices: (e) gelled bioink on fibrin, (f) non-gelled bioink on Matrigel, and (g) gelled bioink on Matrigel.

(Fig. S4b). HUVECs printed on Matrigel showed cord-like self-assembly along the printed line (Fig. 2b). We also observed HUVECs sprouting originating from the main cord-like formation. However, cord-like formations were unstable and started disintegrating 2-days post printing. A random and more stable HUVECs network was formed in a control experiment (Fig. S4c), involving conventional cell seeding on Matrigel. Poor cell adhesion in bioprinted lines might have occurred due to the smaller number of total cells compared to conventional cell seeding. Bioprinting on Matrigel/thrombin matrix resulted in the formation of well-resolved cord-like formations of HUVECs (Fig. 2d). Since the bioink contained fibrinogen and the substrate thrombin, a fibrin layer was formed along the printed lines like printing on fibrin substrates.

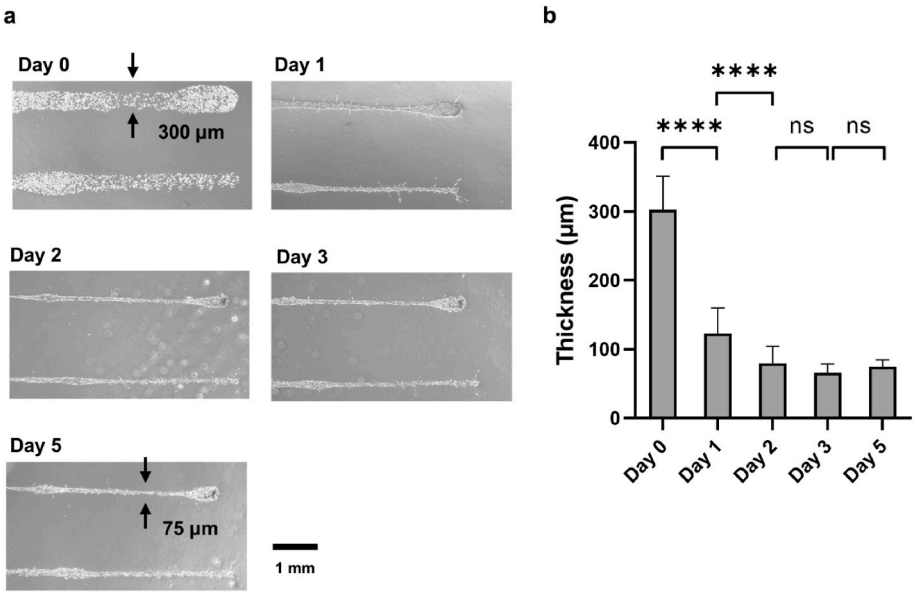

Fig. 3. (a) Optical microscopy images of LIST-printed HUVECs. Drastic self-assembly occurs in day 1. (b) The evolution of LIST-printed lines thickness over time. Error bars represent standard deviation of 5 biological replicates. One-way ANOVA test was used for mean comparison. Significant differences are indicated by asterisks ($P < 0.0001$ = ****).

Although sprouting was observed, those cord-like formations maintained the initial printing geometry. Conversely, HUVECs showed random network formation in a control experiment of conventional cell seeding on Matrigel/thrombin substrate (Fig. S4cd).

These results indicate that the matrix selection plays a predominant role in HUVECs self-assembly for otherwise identical printing conditions. The use of Matrigel/thrombin matrix provides a highly desirable combined effect: strong cell adhesion along the printed lines (fibrin) and poor cell migration towards the outer area (Matrigel/thrombin). Consequently, we selected the Matrigel/thrombin matrix as a platform to study the stability of bioprinted cord-like formations and to assess tubulogenesis.

3.3. LIST-printed HUVECs lines regress with time

To evaluate the evolution of the cord-like formations with time, we measured their thickness up to 5-days post printing. We found that the initial thickness of the structures was 303 ± 48 μm and that it progressively regressed to 75 ± 10 μm 5-days post printing (Fig. 3). Statistically significant regression takes place up to 2-days post printing (from 303 ± 48 μm to 123 ± 37 μm), whereas the size of the structures remains stable past this time point. Given that we did not observe any contraction of the gel (i.e., the initial spacing of the lines was preserved with time), we attribute the thinning of the lines to dense self-assembly of the printed cells. We limited the analysis to 5-days post printing as cord-like formations start to disintegrate starting from 6-days post printing. These results indicate that starting from 2-days post printing HUVECs have completed self-assembly.

3.4. Evaluating the effect of pro- and anti-angiogenic factors on sprouting from LIST-printed patterns

Next, we sought to investigate how anti- and pro-angiogenic factors affect sprouting angiogenesis from the printed lines. We selected two anti-angiogenic (BMP9 and FLT1-FC) and two pro-angiogenic (BMP6 and VEGF) compounds for this study. BMP9 and FLT1-FC were evaluated, as it was previously shown that they elicit potent anti-angiogenic effects in fibrin angiogenesis assays by modulating Alk1 and VEGF signaling respectively [33,37]. Conversely, the effects of VEGF and BMP6 were assessed, as they have been shown to reproducibly promote sprouting angiogenesis in Matrigel and Fibrin HUVEC assays [38]. We first investigated the effect of those compounds using a conventional angiogenesis assay comprised of treating HUVECs seeded on fibrin. For VEGF treatment, we found more junctions and longer network length compared to control (Figs. S5 and S6), whereas BMP6 treatment shows a similar trend. BMP9 and FLT1-FC treatments resulted in a reversed effect (Figs. S5 and S6). These results confirm the anti- and pro-angiogenesis effect of the used compounds.

We applied similar stimulations to printed lines by adding the various compounds in the culture media post printing. We then

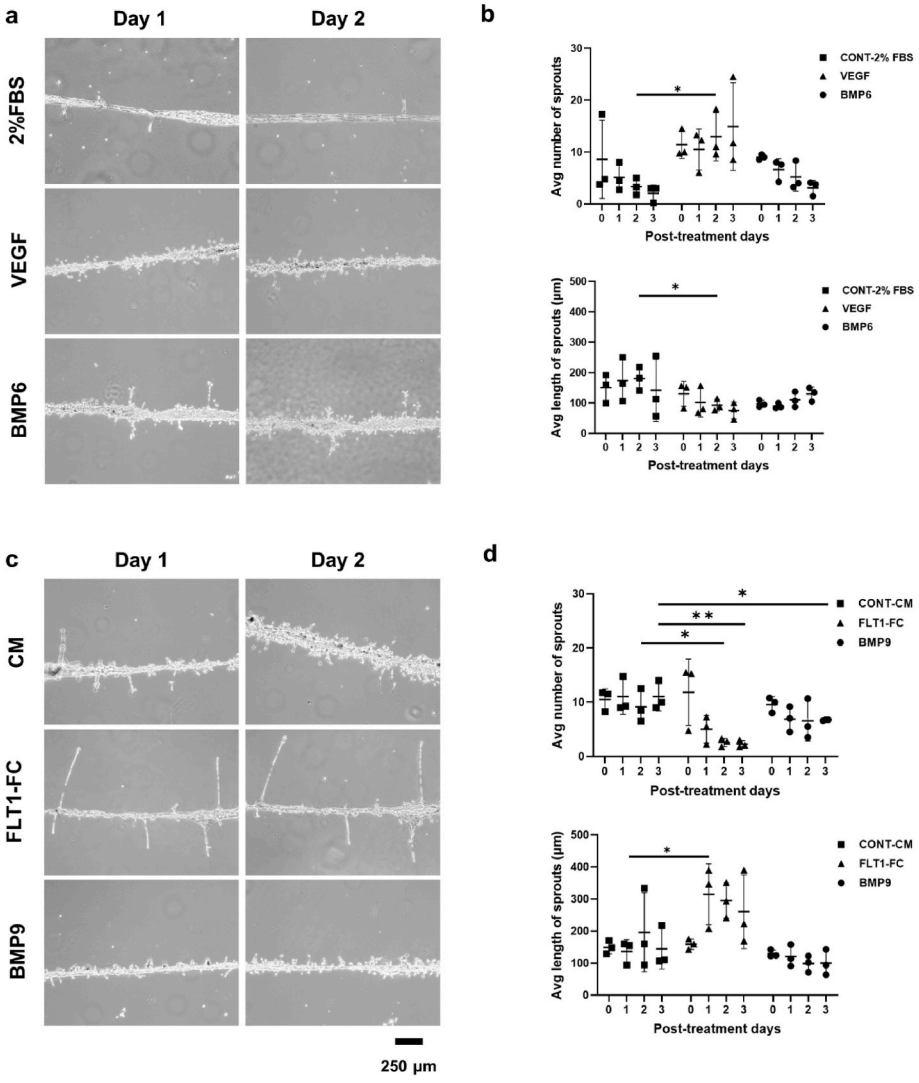

Fig. 4. (a) Bright field microscopy images of HUVECs printed lines treated by pro-angiogenic factors (BMP6 and VEGF) and control media (2% FBS). (b) The average number of sprouts and the average length of sprouts for (BMP6 and VEGF) and control (Basal Media-2% FBS) treatments. (c) Bright field microscopy images of HUVEC-printed lines treated by anti-angiogenic factors (BMP9 and FLT1-FC) and control (Complete Medium (CM)). (b) The average number of sprouts and the average length of sprouts for (BMP9 and FLT1-FC) and control (CM) treatments. Error bars represent standard deviation of 3 biological replicates. Two-way ANOVA test was used for mean comparison. Significant differences are indicated by asterisks ($P < 0.05$ = * and $P < 0.01$ = **).

quantified the length and number of sprouts originating from the cord-like formations of HUVECs. We found a trend of more sprouts for VEGF treatments compared to control (2% FBS) (Fig. 4a and b). We found a reversed trend for the average length of the sprouts for both BMP6 and VEGF treatments (Fig. 4a and b). For 2-days post treatment with VEFG, the differences are statistically significant. For the evaluation of anti-angiogenic compounds (BMP9 and FLT1-FC), cultures were grown in complete ECGM2 medium, which include VEGF, FGF-2 and EGF as growth supplements. For 2- and 3-days post treatment, we found significantly less sprouts for FLT-FC1 treatment (anti-angiogenic), whereas we observed a similar trend for 1-day post treatment. (Fig. 4c and d). We also found significantly less sprouts for BMP9 treatment compared to control for 3-days post treatment, whereas there was a non-significant similar trend for 1- and 2-days post treatment. (Fig. 4c and d). Furthermore, FLT1-FC treatment resulted in longer sprouts 1-day post treatment, whereas a similar trend was observed for 2 and 3-days post treatment. Printed lines cultured in the presence of FLT1-FC also displayed a smoother appearance compared to controls or pro-angiogenic agents, which was likely a consequence of VEGF inhibition, leading to the inhibition of endothelial sprouting and filopodia xtension [39]. Overall, these results are consistent with those obtained from the control assay (Figs. S5 and S6).

3.5. *Evaluating the effects of pro- and anti-angiogenic factors on guided tubulogenesis*

Lumen formation must accompany the de novo growth of blood vessels during angiogenesis. Yet, *in vitro* assays do not always recapitulate this critical step of vascular development; particularly, HUVECs plated in conventional Matrigel assays do not make intercellular lumens, neither sprouting nor proliferation occur [40,41]. As such, we sought to investigate whether a lumen was present in cord-like structures of printed HUVECs and whether pro- and anti-angiogenic factors could affect lumen formation.

Pro-angiogenic (BMP6, VEGF) and anti-angiogenic (BMP9, FLT1-FC) factors were added to the medium 1-day post printing and the treatment was repeated every other day. Given that self-assembled formations remain stable up to 5-days post printing (Fig. 3), we performed immunofluorescence (CD31 and DAPI) imaging at this time point. For all treatments, we found that HUVECs formed intercellular junctions (green staining) and self-assembled in 3D (Fig. 5a–f). Further investigation of cross-sectional images revealed that a partial lumen was formed in the self-assembled patterns and that the different treatments clearly affected the characteristics of the lumen formation. A MATLAB algorithm was developed to quantify the extent of lumen formation. The algorithm quantifies the presence of contained (i.e., surrounded by cells) acellular volume within a printed pattern. We used the algorithm to calculate what fraction of a given line presents complete lumen formation (i.e., length of section(s) with lumen/total length).

We found that BMP9 treatment significantly improved the tubulogenesis process compared to both FLT1-FC and control (Fig. 5a–c, and 5g), consistent with a previous study showing that BMP9 participates in lumen formation and maintenance [42]. Printed lines treated with BMP9 presented complete lumen formation for 46.5% of their length, while lines exposed to complete medium for 18.2% of their length. We found no significant effects for pro-angiogenic treatments (BMP6 and VEGF). However, we did observe a trend of improved tubulogenesis for BMP6, compared to VEGF and control. Taken together these results indicate the LIST-printed HUVECs can self-assemble in 3D and that they can support tubulogenesis in a spatially guided manner. Yet, the lumen formation is partial along the printed structure, while anti-angiogenic treatment (BMP9) significantly improves tubulogenesis compared to complete medium.

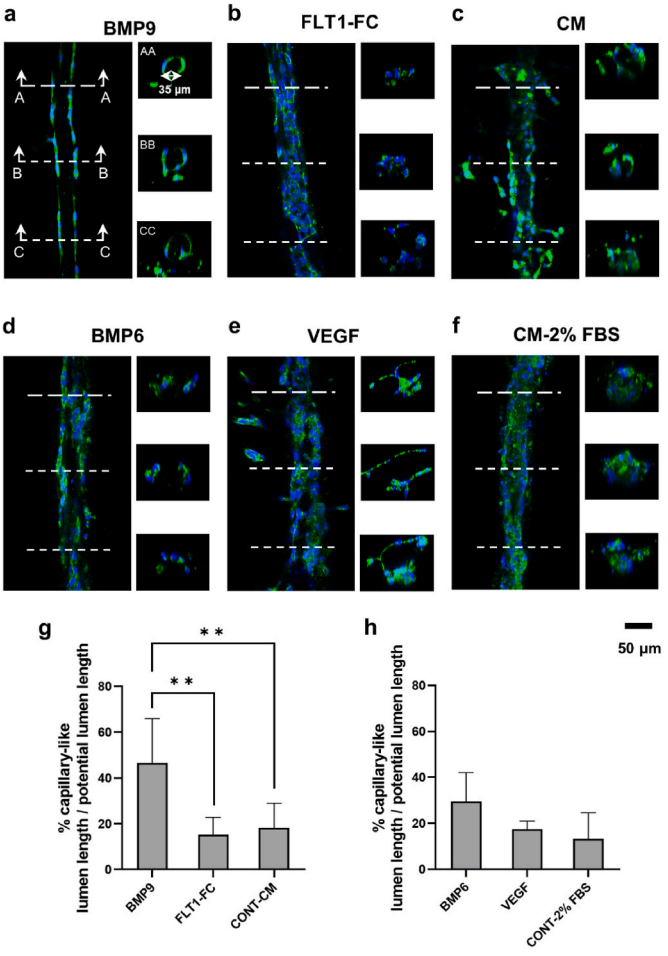

Fig. 5. (a–c) Day 5 confocal microscopy of LIST-printed HUVECs lines including cross sectional views. The lines were treated by anti-angiogenic factors (BMP9 and FLT1-FC) or control (CM). (d–f) Day 5 confocal microscopy of LIST-printed HUVECs lines including cross sectional views. The lines were treated by pro-angiogenic factors (BMP6 and VEGF) or control (Basal Media-2% FBS). Green indicates CD31 and blue indicates cell nuclei staining with DAPI. (g–h) Capillary-like length over potential lumen length for anti-angiogenic factors (BMP9 and FLT1-FC) or CM (g) for pro-angiogenic factors (BMP6 and VEGF) or control (Basal media-2%FBS). Error bars represent standard deviation of 3 biological replicates. One-way ANOVA test was used for mean comparison. Significant differences are indicated by asterisks ($P < 0.01 = **$). (For interpretation of the references to colour in this figure legend, the reader is referred to the Web version of this article.)

4. Discussion

Bioprinting can spatially control tubulogenesis compared to conventional angiogenesis assays. Yet, HUVECs self-assembly and adherence to the matrix should be optimized in bioprinting. In agreement with the literature [40,43,44], our findings on conventional assays show that the HUVECs seeded on fibrin gel form randomly organized networks. Bioprinted HUVECs, initially contained in gelled lines on fibrin, migrate and proliferate without preserving the initial pattern. This behaviour can be attributed to the relatively soft fibrin matrix (Fig. S3). The use of Matrigel as matrix confined HUVECs along the printed lines and promoted self-assembly in cord-like formations. For cells printed on Matrigel, we observed sporadic cell detachment starting from day-2 post printing. This can be attributed to poor cell-cell contacts [45] and/or to the reception of conflicting signaling from Matrigel and initiation of the apoptotic machinery [45]. LIFT bioprinted networks of HUVECs on Matrigel showed similar instability [23].

Matrigel was selected as it provides biochemical and mechanical

signals for the self-assembly of HUVECs following bioprinting by preventing excessive dissemination of endothelial cells. While the potential for xenogenic contaminants in Matrigel or Matrigel-cultured cells may prevent clinical application, several synthetic Matrigel alternatives have been developed, which conserve the performance and properties of Matrigel. Such synthetic alternatives to Matrigel could be used as scaffold for printing endothelial cells for clinical applications [46].

The relatively poor migration potential of HUVECs on Matrigel can be exploited to maintain the initial shape of the printed patterns. To prevent cell detachment of the printed cells, we tested a Matrigel/thrombin substrate. Considering that Matrigel and Matrigel/thrombin matrices have similar mechanical properties (Fig. S3), one can explain the drastic improvement in cell confinement to the formation of fibrin stripes on Matrigel. Note that the addition of thrombin in Matrigel has been also shown to promote tubulogenesis both *in vitro* and *in vivo* [47]. HUVECs undergo rapid self-assembly on Matrigel/thrombin matrix. The lines take their final shape 2-days post printing; however, HUVECs printed lines are unstable and would likely require the supplementation of specific growth factors such as Angiopoietins [40] or TGFbeta [48] or the addition of support cells such as fibroblasts or pericytes to maintain long-term stability. It has been shown that HUVECs co-cultures containing support cells such as pericytes stabilize endothelial cell tube-like structures on Matrigel [48]. The addition of pericytes results in enhanced endothelial tube stability and limit the need for exogenous growth factors. In normal physiology, pericytes are essential for the maturation and stabilization of vasculature, and their dysfunction is associated in a variety of physiological disorders such as tumor angiogenesis [49]. In a variety *in vitro* co-culture, pericytes thus stabilize HUVEC tube networks via both direct cell-cell contacts and paracrine signaling pathways [50]. As such, the addition of support cells such as pericytes on HUVEC printed lines will likely improve the long-term stability of vascular structures and more closely mimic *in vivo* settings.

LIFT has been previously used to pattern HUVECs on various matrices, including collagen hydrogel [26], Collagen Type I and Matrigel impregnated biopapers [25], and Matrigel [23]. In those studies, cord-like structures were observed but lumen formation was not investigated [23,25,26]. Compared to LIFT, LIST bioprinting eliminates the donor preparation complexity. Yet, the spatial resolution in our current LIST setting is 165 μm, which is inferior to that attained by LIFT (10–140 μm) for similar cell types. An approach to improve the spatial resolution in LIST is to use capillaries of smaller size. However, cell printing reliability is yet to be tested using such an implementation. LIST can be modified to enable multiple bioink printing capabilities in both simultaneous and sequential printing schemes. This can be implemented using multiple glass capillaries and/or laser beams. Multiple bioink printing is of particular interest for tissue engineering applications, where multicellular architectures are essential. For instance, microvascular tissue engineering applications can further benefit by LIST co-printing of perivascular cells (i.e., pericytes, smooth muscle cells, fibroblasts) along with HUVECs.

Here, we found partial lumen formation for LIST printed HUVECs. Interestingly, we found that the use of pro- and anti-angiogenic compounds has a profound effect on lumen formation. To the best of our knowledge, the effect of pro- and anti-angiogenic treatments on bioprinted HUVECs patterns has not been previously studied in bioprinted assays. For treatment with the anti-angiogenic factor of BMP9, 46.5 ± 19.4% of the printed lines' length presented a complete lumen formation. Furthermore, BMP9 treated lines showed a uniform circular shape. While the mechanisms by which BMP9 promotes the formation of lumenized vascular structures are unclear, it has previously been reported that BMP9 can facilitate lumen formation in part by decreasing endothelial cell migration in blood vessels [42]. Thus, BMP9 signaling could trigger quiescence and changes in cytoskeletal organization in endothelial cells to enhance tube formation in printed HUVECs. Further improvement of the tubulogenesis can be attained by the printing of other cell types such as smooth muscle cells [23,51], human mesenchymal stem cells (hMSCs) [52] and myoblasts [53] along with the printed HUVECs.

5. Conclusion

In conclusion, we showed spatially controlled endothelial tubulogenesis by LIST bioprinting a HUVECs – laden bioink containing fibrinogen. Central in achieving guided tubulogenesis is the selection of the matrix. We tested fibrin, Matrigel and Matrigel/thrombin matrices and found that HUVECs self-assembly is optimal in Matrigel/thrombin matrices due to the formation of fibrin stripes that enhance HUVECs confinement. Importantly, we found partial lumen formation for printed lines of HUVECs and showed that treatment with the anti-angiogenic factor BMP9 significantly improves the percentage of lumen coverage. By documenting treatment-dependent lumen formation and shape preservation in bioprinted patterns, our results showcase LIST as a powerful bioprinting technology to study tubulogenesis and screen compounds targeting microvasculature pathologies.

CRediT authorship contribution statement

Hamid Ebrahimi Orimi: Conceptualization, Methodology, Software, Formal analysis, Investigation, Data curation, Writing – original draft, Visualization. **Erika Hooker:** Investigation. **Sivakumar Narayanswamy:** Supervision. **Bruno Larrivée:** Conceptualization, Methodology, Formal analysis, Resources, Writing – review & editing, Visualization, Supervision. **Christos Boutopoulos:** Conceptualization, Methodology, Resources, Writing – review & editing, Visualization, Supervision, Funding acquisition.

Declaration of competing interest

The authors declare the following financial interests/personal relationships which may be considered as potential competing interests: Christos Boutopoulos reports financial support was provided by Natural Sciences and Engineering Research Council of Canada (RGPIN-2018-06767). Christos Boutopoulos reports financial support was provided by Fonds de la Recherche en Santé du Quebec (#253123, #265459, #312263). Hamid Ebrahimi Orimi reports financial support was provided by Fonds de recherche du Québec Nature et technologies (#263066).

Data availability

Data will be made available on request.

Appendix A. Supplementary data

Supplementary data to this article can be found online at https://doi.org/10.1016/j.bprint.2022.e00240.

References

[1] I.T. Ozbolat, 3D Bioprinting: Fundamentals, Principles and Applications, 2016.
[2] S.V. Murphy, A. Atala, 3D bioprinting of tissues and organs, Nat. Biotechnol. 32 (2014) 773–785, https://doi.org/10.1038/nbt.2958.
[3] C. Tomasina, T. Bodet, C. Mota, L. Moroni, S. Camarero-Espinosa, Bioprinting Vasculature: Materials, Cells and Emergent Techniques, Mater., Basel, Switzerland, 2019, p. 12, https://doi.org/10.3390/ma12172701.
[4] J. Rouwkema, A. Khademhosseini, Vascularization and angiogenesis in tissue engineering: beyond creating static networks, Trends Biotechnol. 34 (2016) 733–745, https://doi.org/10.1016/j.tibtech.2016.03.002.
[5] R.K. Jain, P. Au, J. Tam, D.G. Duda, D. Fukumura, Engineering vascularized tissue, Nat. Biotechnol. 23 (2005) 821–823, https://doi.org/10.1038/nbt0705-821.
[6] A. Negro, T. Cherbuin, M.P. Lutolf, 3D inkjet printing of complex, cell-laden hydrogel structures, Sci. Rep. 8 (2018) 1–9, https://doi.org/10.1038/s41598-018-35504-2.
[7] J.A. Park, S. Yoon, J. Kwon, H. Now, Y.K. Kim, W.J. Kim, J.Y. Yoo, S. Jung, Freeform micropatterning of living cells into cell culture medium using direct

inkjet printing, Sci. Rep. 7 (2017) 1–11, https://doi.org/10.1038/s41598-017-14726-w.
[8] Y.K. Kim, J.A. Park, W.H. Yoon, J. Kim, S. Jung, Drop-on-demand inkjet-based cell printing with 30-μm nozzle diameter for cell-level accuracy, Biomicrofluidics 10 (2016) 1–11, https://doi.org/10.1063/1.4968845.
[9] H.R. Lee, S.M. Jung, S. Yoon, W.H. Yoon, T.H. Park, S. Kim, H.W. Shin, D. S. Hwang, S. Jung, Immobilization of planktonic algal spores by inkjet printing, Sci. Rep. 9 (2019) 1–7, https://doi.org/10.1038/s41598-019-48776-z.
[10] A.A. Antoshin, S.N. Churbanov, N.V. Minaev, D. Zhang, Y. Zhang, A.I. Shpichka, P. S. Timashev, LIFT-bioprinting, is it worth it? Bioprinting 15 (2019), e00052 https://doi.org/10.1016/j.bprint.2019.e00052.
[11] A. Panwar, L.P. Tan, Current status of bioinks for micro-extrusion-based 3D bioprinting, Molecules 21 (2016), https://doi.org/10.3390/molecules21060685.
[12] J.W. Lee, Y.J. Choi, W.J. Yong, F. Pati, J.H. Shim, K.S. Kang, I.H. Kang, J. Park, D. W. Cho, Development of a 3D cell printed construct considering angiogenesis for liver tissue engineering, Biofabrication 8 (2016), 15007, https://doi.org/10.1088/1758-5090/8/1/015007.
[13] D.B. Kolesky, K.A. Homan, M.A. Skylar-Scott, J.A. Lewis, Three-dimensional bioprinting of thick vascularized tissues, Proc. Natl. Acad. Sci. U.S.A. 113 (2016) 3179–3184, https://doi.org/10.1073/pnas.1521342113.
[14] T.J. Hinton, Q. Jallerat, R.N. Palchesko, J.H. Park, M.S. Grodzicki, H.J. Shue, M. H. Ramadan, A.R. Hudson, A.W. Feinberg, Three-dimensional printing of complex biological structures by freeform reversible embedding of suspended hydrogels, Sci. Adv. 1 (2015), https://doi.org/10.1126/sciadv.1500758.
[15] F. Maiullari, M. Costantini, M. Milan, V. Pace, M. Chirivì, S. Maiullari, A. Rainer, D. Baci, H.E.S. Marei, D. Seliktar, C. Gargioli, C. Bearzi, R. Rizzi, A multi-cellular 3D bioprinting approach for vascularized heart tissue engineering based on HUVECs and iPSC-derived cardiomyocytes, Sci. Rep. 8 (2018) 1–15, https://doi.org/10.1038/s41598-018-31848-x.
[16] L. Xu, M. Varkey, A. Jorgensen, J. Ju, Q. Jin, J.H. Park, Y. Fu, G. Zhang, D. Ke, W. Zhao, R. Hou, A. Atala, Bioprinting small diameter blood vessel constructs with an endothelial and smooth muscle cell bilayer in a single step, Biofabrication 12 (2020), https://doi.org/10.1088/1758-5090/aba2b6.
[17] M.A. Skylar-Scott, S.G.M. Uzel, L.L. Nam, J.H. Ahrens, R.L. Truby, S. Damaraju, J. A. Lewis, Biomanufacturing of organ-specific tissues with high cellular density and embedded vascular channels, Sci. Adv. 5 (2019), https://doi.org/10.1126/sciadv.aaw2459.
[18] W. Jia, P.S. Gungor-Ozkerim, Y.S. Zhang, K. Yue, K. Zhu, W. Liu, Q. Pi, B. Byambaa, M.R. Dokmeci, S.R. Shin, A. Khademhosseini, Direct 3D bioprinting of perfusable vascular constructs using a blend bioink, Biomaterials 106 (2016) 58–68, https://doi.org/10.1016/j.biomaterials.2016.07.038.
[19] D. Takagi, W. Lin, T. Matsumoto, H. Yaginuma, N. Hemmi, S. Hatada, M. Seo, High-precision three-dimensional inkjet technology for live cell bioprinting, Int. J. Bioprinting. 5 (2019) 27–38, https://doi.org/10.18063/ijb.v5i2.208.
[20] M. Yanez, J. Rincon, A. Dones, C. De Maria, R. Gonzales, T. Boland, In vivo assessment of printed microvasculature in a bilayer skin graft to treat full-thickness wounds, Tissue Eng. 21 (2015) 224–233, https://doi.org/10.1089/ten.tea.2013.0561.
[21] O. Kérourédan, D. Hakobyan, M. Rémy, S. Ziane, N. Dusserre, J.C. Fricain, S. Delmond, N.B. Thébaud, R. Devillard, In situ prevascularization designed by laser-assisted bioprinting: effect on bone regeneration, Biofabrication 11 (2019), 45002, https://doi.org/10.1088/1758-5090/ab2620.
[22] J.M. Bourget, O. Kérourédan, M. Medina, M. Rémy, N.B. Thébaud, R. Bareille, O. Chassande, J. Amédeé, S. Catros, R. Devillard, Patterning of endothelial cells and mesenchymal stem cells by laser-assisted bioprinting to study cell migration, 2016, BioMed Res. Int. (2016), https://doi.org/10.1155/2016/3569843.
[23] P.K. Wu, B.R. Ringeisen, Development of human umbilical vein endothelial cell (HUVEC) and human umbilical vein smooth muscle cell (HUVSMC) branch/stem structures on hydrogel layers via biological laser printing (BioLP), Biofabrication 2 (2010), https://doi.org/10.1088/1758-5082/2/1/014111.
[24] R. Gaebel, N. Ma, J. Liu, J. Guan, L. Koch, C. Klopsch, M. Gruene, A. Toelk, W. Wang, P. Mark, F. Wang, B. Chichkov, W. Li, G. Steinhoff, Patterning human stem cells and endothelial cells with laser printing for cardiac regeneration, Biomaterials 32 (2011) 9218–9230, https://doi.org/10.1016/j.biomaterials.2011.08.071.
[25] R.K.R.K. Pirlo, P. Wu, J. Liu, B. Ringeisen, PLGA/hydrogel biopapers as a stackable substrate for printing HUVEC networks via BioLP™, Biotechnol. Bioeng. 109 (2012) 262–273, https://doi.org/10.1002/bit.23295.
[26] O. Kérourédan, J.M. Bourget, M. Rémy, S. Crauste-Manciet, J. Kalisky, S. Catros, N. B. Thébaud, R. Devillard, Micropatterning of endothelial cells to create a capillary-like network with defined architecture by laser-assisted bioprinting, J. Mater. Sci. Mater. Med. 30 (2019), https://doi.org/10.1007/s10856-019-6230-1.
[27] H. Ebrahimi Orimi, S.S. Hosseini Kolkooh, E. Hooker, S. Narayanswamy, B. Larrivée, C. Boutopoulos, Drop-on-demand cell bioprinting via laser induced side transfer (LIST), Sci. Rep. 10 (2020) 9730, https://doi.org/10.1038/s41598-020-66565-x.
[28] K. Roversi, H. Ebrahimi Orimi, M. Falchetti, E. Lummertz da Rocha, S. Talbot, C. Boutopoulos, Bioprinting of adult dorsal root ganglion (DRG) neurons using laser-induced side transfer (LIST), Micromachines 12 (2021) 865, https://doi.org/10.3390/mi12080865.
[29] C. Viallard, C. Audiger, N. Popovic, N. Akla, K. Lanthier, I. Legault-Navarrete, H. Melichar, S. Costantino, S. Lesage, B. Larrivée, BMP9 signaling promotes the normalization of tumor blood vessels, Oncogene 39 (2020) 2996–3014, https://doi.org/10.1038/s41388-020-1200-0.
[30] K.P. Mouillesseaux, D.S. Wiley, L.M. Saunders, L.A. Wylie, E.J. Kushner, D. C. Chong, K.M. Citrin, A.T. Barber, Y. Park, J.D. Kim, L.A. Samsa, J. Kim, J. Liu, S. W. Jin, V.L. Bautch, Notch regulates BMP responsiveness and lateral branching in vessel networks via SMAD6, Nat. Commun. 7 (2016) 1–12, https://doi.org/10.1038/ncomms13247.
[31] H. Ebrahimi Orimi, L. Arreaza, S. Narayanswamy, C. Boutopoulos, Self-limited nanosecond laser-induced bubble growth in sealed containers, Appl. Phys. Lett. 119 (2021), 064101, https://doi.org/10.1063/5.0063048.
[32] B. Herrera, G.J. Inman, A rapid and sensitive bioassay for the simultaneous measurement of multiple bone morphogenetic proteins. Identification and quantification of BMP4, BMP6 and BMP9 in bovine and human serum, BMC Cell Biol. 10 (2009) 20, https://doi.org/10.1186/1471-2121-10-20.
[33] L. David, C. Mallet, S. Mazerbourg, J.-J. Feige, S. Bailly, Identification of BMP9 and BMP10 as functional activators of the orphan activin receptor-like kinase 1 (ALK1) in endothelial cells, Blood 109 (2007) 1953, https://doi.org/10.1182/blood-2006-07-034124. –1961.
[34] N. Akla, C. Viallard, N. Popovic, C. Lora Gil, P. Sapieha, B. Larrivée, BMP9 (bone morphogenetic protein-9)/alk1 (Activin-Like kinase receptor type I) signaling prevents hyperglycemia-induced vascular permeability, Arterioscler. Thromb. Vasc. Biol. 38 (2018) 1821–1836, https://doi.org/10.1161/ATVBAHA.118.310733.
[35] K. Ntumba, N. Akla, S.P. Oh, A. Eichmann, B. Larrivée, BMP9/ALK1 inhibits neovascularization in mouse models of age-related macular degeneration, Oncotarget 7 (2016) 55957–55969, https://doi.org/10.18632/oncotarget.11182.
[36] M. Bland, An Introduction to Medical Statistics, fourth ed., Oxford University Press, 2015.
[37] B. Larrivée, C. Prahst, E. Gordon, R. del Toro, T. Mathivet, A. Duarte, M. Simons, A. Eichmann, ALK1 signaling inhibits angiogenesis by cooperating with the notch pathway, Dev. Cell 22 (2012) 489–500, https://doi.org/10.1016/j.devcel.2012.02.005.
[38] A. Benn, C. Hiepen, M. Osterland, C. Schütte, A. Zwijsen, P. Knaus, Role of bone morphogenetic proteins in sprouting angiogenesis: differential BMP receptor-dependent signaling pathways balance stalk vs. tip cell competence, Faseb. J. 31 (2017) 4720–4733, https://doi.org/10.1096/fj.201700193RR.
[39] H. Gerhardt, M. Golding, M. Fruttiger, C. Ruhrberg, A. Lundkvist, A. Abramsson, M. Jeltsch, C. Mitchell, K. Alitalo, D. Shima, C. Betsholtz, VEGF guides angiogenic sprouting utilizing endothelial tip cell filopodia, J. Cell Biol. 161 (2003) 1163–1177, https://doi.org/10.1083/jcb.200302047.
[40] M.N. Nakatsu, R.C.A. Sainson, J.N. Aoto, K.L. Taylor, M. Aitkenhead, S. Pérez-del-Pulgar, P.M. Carpenter, C.C.W. Hughes, Angiogenic sprouting and capillary lumen formation modeled by human umbilical vein endothelial cells (HUVEC) in fibrin gels: the role of fibroblasts and Angiopoietin-1, Microvasc. Res. 66 (2003) 102–112, https://doi.org/10.1016/S0026-2862(03)00045-1.
[41] D. Donovan, N.J. Brown, E.T. Bishop, C.E. Lewis, Comparison of three in vitro human “angiogenesis” assays with capillaries formed in vivo, Angiogenesis 4 (2001) 113–121, https://doi.org/10.1023/A:1012218401036.
[42] A.-C. Vion, S. Alt, A. Klaus-Bergmann, A. Szymborska, T. Zheng, T. Perovic, A. Hammoutene, M.B. Oliveira, E. Bartels-Klein, I. Hollfinger, P.-E. Rautou, M. O. Bernabeu, H. Gerhardt, Primary cilia sensitize endothelial cells to BMP and prevent excessive vascular regression, J. Cell Biol. 217 (2018) 1651–1665, https://doi.org/10.1083/jcb.201706151.
[43] H. Hall, T. Baechi, J.A. Hubbell, Molecular properties of fibrin-based matrices for promotion of angiogenesis in vitro, Microvasc. Res. 62 (2001) 315–326, https://doi.org/10.1006/mvre.2001.2348.
[44] K.T. Morin, R.T. Tranquillo, In vitro models of angiogenesis and vasculogenesis in fibrin gel, Exp. Cell Res. 319 (2013) 2409–2417, https://doi.org/10.1016/j.yexcr.2013.06.006.
[45] V. Ranta, T. Mikkola, O. Ylikorkala, L. Viinikka, A. Orpana, Reduced viability of human vascular endothelial cells cultured on matrigel, J. Cell. Physiol. 176 (1998) 92–98, https://doi.org/10.1002/(SICI)1097-4652(199807)176:1<92::AID-JCP11>3.0.CO;2-Q.
[46] E.A. Aisenbrey, W.L. Murphy, Synthetic alternatives to matrigel, Nat. Rev. Mater. 5 (2020) 539–551, https://doi.org/10.1038/s41578-020-0199-8.
[47] G.C. Haralabopoulos, D.S. Grant, H.K. Kleinman, M.E. Maragoudakis, Thrombin promotes endothelial cell alignment in Matrigel in vitro and angiogenesis in vivo, Am. J. Physiol. Cell Physiol. 273 (1997), https://doi.org/10.1152/ajpcell.1997.273.1.c239.
[48] D.C. Darland, P.A. D'Amore, TGF beta is required for the formation of capillary-like structures in three-dimensional cocultures of 10T1/2 and endothelial cells, Angiogenesis 4 (2001) 11–20, https://doi.org/10.1023/a:1016611824696.
[49] A.P. Hall, Review of the pericyte during angiogenesis and its role in cancer and diabetic retinopathy, Toxicol. Pathol. 34 (2006) 763–775, https://doi.org/10.1080/01926230600936290.
[50] H. Zhao, J.C. Chappell, Microvascular bioengineering: a focus on pericytes, J. Biol. Eng. 13 (2019) 26, https://doi.org/10.1186/s13036-019-0158-3.
[51] K.J. Oh, H.S. Yu, J. Park, H.S. Lee, S.A. Park, K. Park, Co-culture of smooth muscle cells and endothelial cells on three-dimensional bioprinted polycaprolactone scaffolds for cavernosal tissue engineering, Aging Male 23 (2021) 830–835, https://doi.org/10.1080/13685538.2019.1601175.
[52] C. Piard, A. Jeyaram, Y. Liu, J. Caccamese, S.M. Jay, Y. Chen, J. Fisher, 3D printed HUVECs/MSCs cocultures impact cellular interactions and angiogenesis depending on cell-cell distance, Biomaterials 222 (2019), 119423, https://doi.org/10.1016/j.biomaterials.2019.119423.
[53] M. Yeo, G.H. Kim, Micro/nano-hierarchical scaffold fabricated using a cell electrospinning/3D printing process for co-culturing myoblasts and HUVECs to induce myoblast alignment and differentiation, Acta Biomater. 107 (2020) 102–114, https://doi.org/10.1016/j.actbio.2020.02.042.